PUBLICATION

MUSTANG

A MUltiple Space and Time scale Approach for the quaNtification of deep saline formations for CO_2 storaGe

Project Number:227286

AUTHORS: *Zhibing Yang, Auli Niemi, Liang Tian, Saba Joodaki, Mikael Erlström*

TITLE: *Modeling of pressure buildup and estimation of maximum injection rate for geological CO2 storage at the South Scania site, Sweden*

The research leading to these results has received funding from the European Community's Seventh Framework Programme [FP7/2007/2013) under grant agreement n° [227286]

Status	AUTHOR VERSION
Date	2014
Publisher	Wiley Online Library
Reference	Greenhouse Gases: Science and Technology, 2014

Modeling of pressure buildup and estimation of maximum injection rate for geological CO_2 storage at the South Scania site, Sweden

Zhibing Yang [1 *] , Auli Niemi [1] , Liang Tian [1] , Saba Joodaki [1] , and Mikael Erlström[2]

[1]Department of Earth Sciences, Uppsala University, Villavägen 16, SE-752 36 Uppsala, Sweden

[2]Geological Survey of Sweden, Kiliansgatan 10, SE-223 50 Lund, Sweden

*Correspondence to zhibing.yang@hyd.uu.se

Abstract. Carbon dioxide (CO_2) injection in deep saline formations causes pressure increase which may be detrimental to the mechanical integrity of the storage reservoir. Injection induced pressure buildup is a limiting factor for CO_2 injection rates and storage capacity. In this study, we extend a semi-analytical solution (based on one-dimensional, two-phase, two-component radial flow) for application to estimate pressure buildup and maximum injection rate of CO_2 at a field site (South Scania, Sweden) using the method of superposition of image well solutions to account for the straight-line boundaries imposed by three fault zones. The semi-analytical approach for estimating pressure buildup is validated by comparison to numerical simulations based on TOUGH2-ECO2N. We analyze injection pressure sensitivity due to uncertainty in reservoir parameters as well as boundary conditions. Maximum injection rates and pressure limited capacity estimates are presented. This work demonstrates the use of semi-analytical solutions to analyze pressure limitation on storage capacity for realistic reservoirs with irregular (non-circular) boundaries. It is also shown that the semi-analytical approach can also be used to evaluate the benefit of having multiple injection wells in terms of increasing the injection-pressure-limited storage capacity. The methodology presented in this study is useful for screening analysis of storage sites as well as for operation design and optimization where pressure buildup as a limiting factor influences the objective function.

Keywords: Geological storage; Pressure-limited capacity; Numerical modeling; Analytical solution; Mechanical failure.

1. Introduction

Reduction of atmospheric greenhouse gas concentrations can be achieved by carbon capture and storage (CCS). Implementation of CCS requires sequestrating a large amount of carbon dioxide (CO_2) preferably in the deep saline formations. For closed formations, the pore space needed for storing CO_2 is accommodated by enlargement of the rock pore space and at the same time reduction in the volume of the formation fluid, through compression of the rock material and the formation fluid, respectively. [1] For semi-closed or open formations, pore space accommodation of the injected CO_2 can be further facilitated by the displacement of the native fluid from the storage formation into overlying and underlying layers through brine leakage or into regions far away from the injection zone. Pore space for storing CO_2 can be even created by production of the native fluid. In any case, pressure perturbation in the host formation will be induced by commercial scale geological storage of CO_2. This can result in direct adverse impact on the mechanical integrity of the storage formation or may even have major secondary effects of concern on the near-surface (fresh water) aquifers. Specifically, injecting a large volume of CO_2 induces large scale pore pressure buildup and associated change in the stress status, which may become a limiting factor for the CO_2 storage capacity because (i) tensile or shear failure of the caprock may take place, (ii) existing fractures and faults may be reactivated, and (iii) large-scale brine displacement into fresh-water aquifers or brine leakage through abandoned well or fault zones may be induced, even if the injected CO_2 is safely trapped. Birkholzer and Zhou [2] argued that the basin-scale hydrogeological impacts (i.e., due to pressure buildup and brine displacement, and associated impacts on the environment) should be taken into account for the regional and

global capacity estimation, which typically has been based on simple calculation of the fraction of the total reservoir pore space. [3] In this study, we focus on modeling and analyzing the pressure buildup that imposes restrictions of the injection rate due to potential mechanical failure and the implication for capacity estimates.

Together with CO_2 injection and plume migration, pressure buildup in a storage formation due to injection can be analyzed through numerical modeling using general three-dimensional multiphase flow simulators such as TOUGH2-ECO2N [4-6] and PFLOTRAN. [7] For example, Zhou et al. [8] performed numerical modelling for CO_2 injection in the Mount Simon aquifer in the Illinois Basin using the parallel version of the TOUGH2 simulator. They simulated CO_2 injection at a rate of 5Mt/year/well with a total number of 20 wells, and found that the simulated pressure buildup in the core injection area is about 35 bars which is not expected to affect the caprock geomechanical integrity. Yamamoto et al. [9] conducted high resolution numerical simulations for CO_2 storage in the Tokyo Bay with a special focus on the large-scale pressure perturbation and the associated shallow subsurface groundwater migration. Their results suggest that groundwater pressure in the shallow confined aquifers can increase a few bars over extensive regions. Birkholzer et al. [10] numerically investigated the fluid pressure response to CO_2 injection in a generic stratified system and concluded that large-scale pressure change has more impact on groundwater resources than changes in water quality caused by the migration of displaced brine. The above studies have employed full hydrodynamic modelling and taken into account both the plume- and basin-scale processes related to CO_2 injection, which requires a significant amount of computational resources. For evaluation of large-scale impact of pressure perturbation, simpler and computationally

less expensive numerical models can also be used. These models include vertically integrated two-phase flow numerical models [11,12] and single-phase numerical models. [13-15] Recent studies have also compared the performance of the numerical models of varying levels of complexity. [14,16,17] It has been shown in these studies that single-phase numerical models may be adequate for prediction of large-scale pressure perturbation and assessment of the area of review. However, when the possible mechanical failure is of concern, single-phase models will lead to considerable inaccuracy in the estimation of pressure change near the injection well due to the significant viscosity ratio between supercritical CO_2 and brine and the evolution of dry-out zone and two-phase flow zone.

In contrast to numerical models, analytical methods allow for rapid evaluation and can be employed to study parameter sensitivity for quick site screening and characterization. Semi-analytical solutions [1,18-22] have been developed to solve the radially symmetric two-phase flow equations for CO_2 saturation and pressure distribution. Each of the analytical methods involves a different set of simplifying assumptions. Some of the usual assumptions include radially symmetrical domain, no-flow top and bottom boundary, negligible capillary pressure, incompressible and immiscible flow, constant fluid and rock properties, linear relative permeability functions etc. Since the compressibility of CO_2 can be one or two orders of magnitude larger than that of brine for typical injection depth, the assumption of constant CO_2 density may lead to notable errors in the calculation of pressure evolution and CO_2 plume shape. In the models of Vilarrasa et al., [21,22] CO_2 compressibility was explicitly accounted for, which is advantageous. The considerable variation of CO_2 properties (i.e., density, viscosity etc.) due to fluid pressure evolution may alternatively be remedied by calculating the fluid properties based on the

equations of state using the final pressure. This can be done by a simple iterative procedure. Mathias et al. [19] presented an analytical solution of pressure buildup taking into account the effect of closed lateral boundary and partial miscibility between CO_2 and brine, ignoring vertical flow of CO_2. It was found that the effect of brine evaporation can be considerable while the effect of CO_2 dissolution is small. Mathias et al. [23] investigated the sensitivity of estimating maximum sustainable injection rate to uncertain non-linear relative permeability parameters.

The CO_2 injection is restricted by the maximum allowable pressure buildup (i.e., the critical pressure buildup to induce tensile failure or fault reactivation), accurate determination of which requires large-scale numerical modeling of the coupled hydromechanical (HM) behaviour. [24-28] Coupled HM modeling also needs detailed data on mechanical properties of rock units. In many cases of site screening and characterization, however, this detailed information may not be available and simplified analysis for the maximum sustainable injection pressure can be performed. [29]

In this paper, we will use both numerical modeling (based on TOUGH2-ECO2N) and a semi-analytical solution (extended from Mathias et al.) [19,23] to investigate the near-well pressure buildup and thus the maximum allowable injection rate under different injection scenarios for the South Scania site, south Sweden. We will also test injection pressure sensitivity due to uncertainty in fluid and rock parameters as well as boundary conditions. Maximum injection rates and pressure limited capacity estimates based on the modeling results will be presented.

2. Methods

In this section, we describe two hydrodynamic modeling methods for pressure buildup, one based on numerical modeling and the other based on a semi-analytical solution. We also provide descriptions on how we estimate the maximum sustainable injection pressure and the maximum injection rate.

2.1. Numerical modeling

Injection and migration of CO_2 into brine formations present a two-phase flow problem. In this study, numerical simulations are conducted using the multiphase flow simulator TOUGH2 [4] with the equation-of-state module ECO2N. [5] ECO2N is a fluid property module designed for applications to geologic sequestration of CO_2 in saline aquifers. It describes the thermodynamics and thermophysical properties of H_2O - NaCl - CO_2 mixtures, and accurately reproduces fluid properties for the temperature, pressure and salinity conditions of interest for geological sequestration. Local equilibrium solubility is applied to treat phase partitioning between the aqueous and the CO_2-rich phase as well as to handle dissolution or precipitation of salt. For details of the numerical model, refer to the manuals. [4,5]

2.2. Analytical methods for pressure buildup

The analytical modeling approach for pressure buildup in this study is based on the semi-analytical solution developed by Mathias et al. [19,23] Here, we extend the solution by including superposition of pressure response from imaginary image wells to take into account the effect of the fault boundaries. Strictly speaking, the approach of superposition is limited to linear systems. This requirement is not satisfied in the two-phase region

where CO_2 and brine coexist. However, as will be shown later, the two-phase region is small compared to the extent of the pressure response, which justifies the use of the superposition approach.

Under reservoir conditions, supercritical CO_2 can partially dissolve into brine and at the same time water can partially vaporize in the presence of CO_2. This partial miscibility gives rise to complex flow regimes and dynamics for the evaluation of pressure response. Assuming vertical pressure equilibrium, constant fluid properties, negligible capillary pressure and equilibrium dissolution between CO_2 and water, Mathias et al. [19] solved the relevant (radially symmetric) governing equations describing the above flow characteristics. It is possible to obtain closed-form solutions for the gas saturation and pressure for the case with linear relative permeability functions. For nonlinear relative permeability functions, numerical evaluation of the gas saturation at the leading shock front needs to be used, and the solution becomes semi-analytical. Note that wellbore skin effect is not considered.

The analytical model [19] can be applied to both laterally open and closed aquifers. It can be summarized as:

$$\Delta P = P - P_{ini} = \frac{M_0}{4\pi\rho_g Hk}\begin{cases}\mu_g q_{D1}\ln(z_T/z)/k_{rs} + \mu_g q_{D2}F_2(z_T) + \mu_b q_{D3}F_1(z_L), & 0 \le z < z_T \\ \mu_g q_{D2}F_2(z) + \mu_b q_{D3}F_1(z_L), & z_T \le z < z_L \\ \mu_b q_{D3}F_1(z), & z \ge z_L\end{cases} \quad (1)$$

where ΔP is the pressure buildup,

P is the vertically averaged pressure,

P_{ini} is the initial pressure (vertically averaged),

M_0 is the mass injection rate of CO_2,

ρ_g is the density of CO_2,

μ_g is the viscosity of CO_2,

k is the permeability of the formation,

H is the thickness of the formation,

k_{rs} is the permeability reduction factor due to salt precipitation,

μ_b is the viscosity of the brine,

q_{D1}, q_{D2}, and q_{D3} are the dimensionless, piecewise total fluxes, which can be obtained from Equations (27) and (28) in Mathias et al. [19]

z is the similarity transform variable for time t and radial distance r

$$z = \frac{\pi\phi\rho_g H r^2}{M_0 t},$$

and z_T and z_L are locations of the trailing and leading shocks in similarity space, which can be evaluated from Equations (30-35 and 53) in Mathias et al. [19]. In Equation (1), $0 \le z < z_T$ correponds to the dry-out zone in physical space; $z_T \le z < z_L$ corresponds to the two-phase region where CO_2 and brine coexist; and $z > z_L$ corresponds to the single-phase region occupied by the native brine. The solution for pressure response reduces to one that is based on single-phase flow when the radial distance r is larger than the extent of CO_2 plume (i.e., $z > z_L$).

In Equation (1),

$$F_1(z) = \begin{cases} (\alpha z_E)^{-1} - \frac{3}{2} + \ln\left(\frac{z_E}{z}\right) + \frac{z - z_L}{z_E}, & z_E < \frac{0.5615}{\alpha} \\ E_1(\alpha z), & z_E > 0.5615/\alpha \end{cases} \quad (2)$$

with

$$\alpha = \frac{M_0 \mu_b (c_r + c_b)}{4\pi \rho_g H k}, \quad (3)$$

$$F_2(z) = -\frac{1}{\mu_g} \int_z^{z_L} \left(\frac{k_{ra}}{\mu_b} + \frac{k_{rg}}{\mu_g} \right)^{-1} \frac{1}{z} dz \quad (4)$$

where ρ_b is the density of the native brine,

z_E is similarity transform for the radial extent of the formation r_E,

k_{ra} and k_{rg} are the relative permeabilities of the aqueous phase and gas phase, respectively,

and c_r and c_b are the compressibilities of rock pores and brine, respectively.

Note that the fluid densities, viscosities and mass fractions in each phase are all functions of pressure and thus vary as pressure builds up in the formation. For estimating pressure buildup, these parameters need to be iteratively determined. In this study, we iteratively solve for pressure buildup by using Equation (1) and updating the parameters based on the equations of state for CO_2 and brine offered in ECO2N which uses the Altunin [30] correlation implemented as a look-up table.

To account for the effect of closed formation boundaries, we calculate the additional pressure increase due to the no-flow boundaries by introducing image wells. The image wells (fictitious injection wells), having the same injection rate M_0 as the real injection well, are placed at locations to create symmetry along no-flow boundaries in the flow field of fictitious unbounded reservoir. The additional pressure increase (ΔP_f) is calculated as:

$$\Delta P_f = \sum_{i=1}^{n_{im}} \Delta P_i(r_i, t) \quad (5)$$

where n_{im} is the number of image wells, and $\Delta P_f(r_i,t)$ is the pressure buildup contribution (calculated by Equation 1) from the *i*th image well with a distance r_i from the actual injection well.

If we consider multiple real injection wells distributed over a modeling domain, the pressure perturbation from each well will interfere with that from the surrounding wells. As a result, the wells that are not close to the open domain boundaries will effectively behave as if they were surrounded by a no-flow boundary. Therefore, in the modeling of pressure buildup in the vicinity of the injection wells, we consider a closed domain for each individual injector with an equivalent domain radial extent r_E determined by the total domain area A and the number of injection wells n_w, that is, $r_E=(A/\pi n_w)^{0.5}$.

2.3. Maximum sustainable injection pressure

Accurate estimation of the maximum sustainable injection pressure (or the injection pressure threshold, P_{th}) would require detailed knowledge of *in situ* stresses and couple flow/mechanical numerical modeling. Due to the lack of information of the stress status for the study site, we resort to simplified analysis to obtain the maximum sustainable injection pressure P_{th}, similar to Rutqvist et al. [26] and Mathias et al. [29] We estimate the initial vertical stress from the weight of the overburden rock, assuming an average saturated rock density of 2260 kg/m^3. This gives an initial vertical stress σ_z = 3.77×10^7 Pa at a depth of 1700 m. We consider two initial stress regimes: an extensional stress regime with stress ratio between the minimum horizontal stress and the vertical stress σ_h /σ_z = 0.7 and a compressional stress regime with σ_h /σ_z = 1.5. For the case of σ_h /σ_z = 0.7, according to Mathias et al., [29] the threshold pressure is constrained by the fracturing pressure, which can be conservatively estimated as the minimum principle stress (i.e., P_{th}

= $0.7\sigma_z$). For the case of $\sigma_h / \sigma_z = 1.5$, the fracturing pressure can be estimated to be equal to σ_z, while the critical pressure for slip (shear failure), P_s, assuming zero cohesion and a friction angle of 30°, can be estimated from the Coulomb failure criterion as [26]

$$P_s = \sigma_{m2} - 2|\tau_{m2}| \quad (6)$$

where σ_{m2} and τ_{m2} are the two-dimensional mean stress and maximum shear stress in the (σ_h, σ_z) plane. This give a slip pressure $P_s = 0.75\sigma_z$, which is smaller than the fracturing pressure and defines the pressure threshold P_{th} in this case. From the above analysis, we can see that the pressure threshold may be determined by different failure modes under different initial stress conditions. However, for the two cases of $\sigma_h / \sigma_z = 0.7$ and 1.5, the threshold pressure only differs to a small extent ($0.7\sigma_z$ and $0.75\sigma_z$). Thus, in this study, we conservatively choose a threshold pressure value equal to $0.7\sigma_z$ which serves to determine the maximum injection rate (M_{max}). This corresponds to a pressure of 2.64×10^7 Pa, or a 55% increase from the initial hydrostatic pressure 1.7×10^7 Pa.

3. The South Scania site, Sweden

We apply the modeling methods to the South Scania site, which is located in the southwestern region of Sweden (see Fig. 1). A number of deep boreholes have been drilled and several sandstone layers have been identified which constitute potential candidates for geological storage of carbon dioxide. [31] These sandstone layers appear in the Lower Cretaceous and Lower Jurassic sequences. In this study, we consider a storage reservoir consisting of these layers (alternating sandstone and siltstone) within the depth interval between 1650 m and 1725 m. The reservoir is bounded by three faults: the Romeleåsen Fault Zone, the Svedala Fault and the Öresund Fault. These faults are conceptualized into straight lines and shown in red in Fig. 1. The boundary conditions

associated with these faults are currently uncertain. However, available geological information indicates that the Romeleåsen Fault is a regional complex system of reverse faults limiting the sedimentary basin, i.e., the Danish Basin to the northeast. The fault zone is, based on lithological and structural data, considered to provide a closed boundary condition for the Lower Cretaceous and Lower Jurassic reservoirs. In this study, we will examine the effect of boundary conditions on the pressure buildup. We assume a uniform thickness for the reservoir and impermeable overlying and underlying formations. The modeling is simplified to the case of a two-dimensional (vertically integrated) numerical analysis. Based on the available site data, we assume a homogeneous permeability of 1.0×10^{-13} m^2 and a porosity of 0.15. The pore compressibility is taken as 4.5×10^{-10} Pa^{-1}. Since there is no site specific data on the capillary pressure and relative permeability parameters, we choose the relevant parameters based on the Mt. Simon sandstones measured by Krevor et al. [32] We use the Brooks-Corey function [33] for capillary pressure and the Brooks-Corey-Burdine function [33,34] for relative permeability. Residual brine saturation S_{wr} is taken as 0.22; residual gas saturation S_{gr} is 0.2; entry capillary pressure is 4600 Pa; and the pore size distribution parameter is 0.55. A study on the effect of heterogeneity on fluid migration and upscaling based on the South Scania site is presented in Yang et al. [35] However, the effect of heterogeneity on pressure buildup will not be discussed here. A more detailed description of the site can be found in Erlström et al. [36]

4. Results

In this section, we first show comparison between the pressure buildup prediction from the TOUGH2-ECO2N simulations and from the semi-analytical solution. Then we

proceed to apply the semi-analytical solution to investigate the effect of operational parameters (such as the number of injection wells) and boundary conditions, followed by sensitivity of pressure prediction to intrinsic reservoir parameters (such as porosity, permeability, rock compressibility, reservoir thickness, etc.). Note that the pressure increase refers to the difference between injection pressure and initial hydrostatic pressure at end of the injection period (50 years), unless otherwise stated.

4.1. Comparison between numerical simulation and semi-analytical solution

In order to validate the semi-analytical approach, we have numerically simulated pressure response due to CO_2 injection in the formation for comparison. We assume closed lateral boundaries imposed by the three fault zones. This boundary condition corresponds to the case of highest possible pressure buildup in the formation because there is no pressure dissipation induced by brine migration out the reservoir. Single well injection at the location of FFC-1 has been modeled. Injection time is set as 50 years. Injection rates ranging from 0.5 to 3.0 Mt/yr have been tested. The simulated CO_2 plume for injection rate of 2.0 Mt/yr has a radius about 3 km, which is much smaller than the flow domain with equivalent radius of 30 km. This also supports the use of the superposition approach for pressure response. Since we focus on the pressure buildup around the injection well, the CO_2 plume plots will not be shown and discussed. Fig. 2 shows the simulated pressure increase in the modeling domain for two injection rates. When the injection rate is 1.0 Mt/yr, the pressure increase at the injection area is 63 bars; when the injection rate is 2.0 Mt/yr, it grows to 120 bars. This almost linear behavior suggests that the two-phase flow region (in between the dry-out zone and the single-phase brine flow zone) does not impose significant non-linearity to the injection rate-

pressure response relationship, probably due to the fact that the two-phase region is much smaller than the extent of the entire flow domain.

In this case of closed reservoir, we have two alternatives to apply the semi-analytical solution. One is to conceptualize the reservoir into a disc shape with an equivalent radius extent r_E for the reservoir based on the area. This yields an equivalent r_E of 30 km. The other is to use superposition of image well solutions to represent the effect of closed boundary conditions. The principle for placement of image wells is to create a fictitious unbounded domain whose flow field has symmetry along the no-flow fault boundaries. It should be noted that, for several linear faults intersected at arbitrary angles, finding the appropriate number of locations of image wells can be a non-trivial task. Some examples of how to consider image wells can be found in Ferris et al. [37] In this study, we consider both primary and secondary image wells to take into account the effect of three fault boundaries (Fig. 3a). Fig. 3b shows that the semi-analytical approach based on superposition of image well solutions can reasonably well match the pressure prediction based on numerical modeling. But there is appreciable differences between the semi-analytical approach with area-equivalent reservoir radial extent and the numerical results; when the injection rate is 1.5 Mt/yr, the pressure increase predicted by equivalent r_E semi-analytical method shows a 14% deviation from the numerical counterpart. The reason for this deviation is due to the fact that the actual distances from the injection well to the boundaries are much smaller than the equivalent r_E of 30 km (the reservoir is significantly non-circular shaped) so that a portion of the reservoir space is not effectively used for pressure dissipation.

From this comparison analysis, it is evident that the semi-analytical method with superposition of image well solutions can give adequate pressure prediction for a site with linear fault boundaries. In the following, we will only use the analytical method for modeling pressure buildup.

4.2. Number of injection wells

Number and locations of injection wells can be characterized as operational parameters for deployment of large-scale CO_2 storage. They can have a significant impact on the magnitude and spatial distribution of pressure buildup, because of which they should be taken into account for optimal design of effective pressure management and thus storage efficiency. In this section, we focus on the effect of number of injection wells on the pressure buildup. To illustrate this, we assume closed boundaries for the three faults, which corresponds to the boundary case of highest pressure buildup. We also assume that wells are located in the center of each part of the divided reservoir domain. Each small part is conceptualized to have an area-equivalent radial extent, $r_E = (A/\pi n_w)^{0.5}$, for simplicity. Fig. 4 shows a schematic illustrating the scenario of multiple injection wells.

Pressure buildup for four different numbers of injection wells (n_w = 1, 3, 5 and 9) is analyzed. Fig. 5 shows that the effect of the number of injectors on the well pressure buildup is strongly dependent on the reservoir permeability. For low permeability (k = 50 mD), there is significant difference in well pressure between the single-well scenario and nine-well scenario for the same total injection rate ($M_{tot} = M_0 \times n_w$). The maximum injection rate M_{max} for the single-well scenario is about 0.98 Mt/yr, whereas for the nine-well scenario, M_{max} increases by a factor of more than 3 (3.2 Mt/yr). When the base-case permeability (k = 100 mD) is considered, M_{max} increases by a factor of about 2.2 from the

case of n_w = 1 to the case of n_w = 9. When permeability is high (k = 400 mD), as shown in Fig.5c, distributing the total injection rate to a larger number of injector does not seem to decrease the well pressure buildup significantly. This is because the spatial distribution of pressure buildup is more uniform (pressure perturbation travels farther, i.e., stronger pressure interaction among different injection wells) when the permeability is higher.

From the above analysis, it can be seen that we can achieve a rate of at least 3 Mt/yr if we have 9 wells, no matter the permeability is 50 or 400 mD. However, more injection wells also require more operational cost for pipeline network, CO_2 transportation, drilling cost, etc. Under the pressure-limited scenario, less injection wells are needed for a higher reservoir permeability when the same amount of CO_2 is to be stored.

4.3. Effect of boundary conditions

The hydraulic properties and boundary conditions along the faults are not exactly known. In order to assess the effect of boundary conditions on pressure buildup prediction, we consider two extreme cases (one for all closed faults and the other for all open faults) together with the case of only one closed fault (Romeleåsen). For the South Scania site, by *open faults* it is meant that the formation continuity is not affected by the faults and that the physical boundary for the reservoir would be at places where the formation pinches out or outcrops. The two extreme cases provide a theoretical bound for pressure buildup prediction for a given reservoir parameter set. We consider one injection well at the location of FFC-1 and we use the semi-analytical method with superposition of image well solutions to account for the effect of boundaries.

Fig. 5 shows that for the base case parameters listed in Sect. 3, the boundary conditions can have a significant impact on the pressure buildup at the injection location. In terms of

the maximum allowed injection rate, the all-closed-faults case corresponds to a rate of 1.6 Mt/yr, while the number for the all-open-faults case is 2.7 Mt/yr. The case of all closed faults decrease the injectivity by about 40% compared to the open boundary case. Fig.2 also shows that the pressure disturbance at the boundaries is significant at 50 years. In fact, the time for the pressure disturbance to reach the boundary can be estimated by $t_{pb} = L^2/4D_h$, where L is the distance from the injection well to boundary and D_h is the hydraulic diffusivity, $D_h = k/\phi\mu_b(c_r + c_b)$. For the parameters given in Sect. 3 and a distance of 25 km, t_{pb} is only about 4 years, much shorter than the injection period of 50 years. If the hydraulic diffusivity is smaller (e.g., by reducing permeability), the boundaries would have less impact on the pressure buildup.

4.4. Sensitivity to intrinsic reservoir parameters

Even though rock properties (parameters) relevant to CO_2 injection and migration can be estimated from field tests and laboratorial experiments on core samples, they can still be considered to a large extent uncertain due to the typical existence of multi-scale heterogeneity. [38,39] The uncertainty of pressure buildup prediction due to relative permeability parameters has been analyzed by Burton et al. [40] and Mathias et al. [23] In this work, we perform sensitivity study of pressure buildup on parameters including permeability, porosity, compressiblity and reservoir thickness. We do this for two sets of boundary conditions: the more probable case of only one impermeable fault (Romeleåsen) according to available geological information and the unfavorable case of all closed boundaries. One injection well at the FFC-1 location is considered. The method of superposition of image well solutions is used. Note that when we vary a parameter we fix all the other parameters to the base case values as specified in Sect. 3.

Formation permeability is the most sensitive parameter for pressure buildup for the case of single injection well. Fig. 7 shows that the pressure increase exhibits a wide range of values as permeability varies for both boundary scenarios. For example, in Fig. 7a, the pressure increase changes from 25 to 253 bars as permeability decrease from 400 to 25 mD for an injection rate of 2 Mt/yr. In comparison to permeability, porosity is a much less sensitive parameter for the pressure buildup. Additionally, the effect of porosity on pressure is dependent on the boundary conditions, as shown in Fig. 8. In the boundary scenario of only one impermeable fault (Fig. 8a), varying porosity leads to negligible effect on pressure increase. This is partly due to the fact that realistic porosity variation is typically small, within a factor of 2 or 3. The other part of the explanation can be argued by the double roles of porosity on injection pressure buildup. For open reservoirs or nearly open reservoirs (such as the one here with one impermeable fault), decreasing porosity means less pore volume available for the compressibility (storativity) effect, but at the same time it also increases hydraulic diffusivity and thus promotes outwards migration of far-field brine. Fig. 8b shows that for the scenario of closed boundaries, porosity can affect the pressure buildup. This is because the far-field migration of brine is limited by the boundaries and the compressibility effect becomes visible. We expect the effect of reservoir rock compressibility to play a similar role to that of porosity. However, rock compressibility will typically have a larger variability than porosity. Fig. 9 presents the effect of rock compressibility on the pressure increase with the compressibility varies from 4.5×10^{-9} Pa^{-1} to 4.5×10^{-11} Pa^{-1}. The effect of reservoir thickness on pressure buildup is presented in Fig. 10. As expected from the semi-analytical solution, pressure increase is inversely proportional to the reservoir thickness.

4.5. Maximum injection rate and pressure limited capacity

Based on the parametric sensitivity study, we determine maximum injection rates for the different parameter sets by assigning a maximum allowable pressure increase of 94 bars (see Sect. 2.3) and looking up in the response of pressure increase to different injection rates. Table 1 summarizes the results of maximum injection rates. In accordance with the pressure buildup results, the maximum injection rate is most sensitive to permeability variations and relatively insensitive to porosity variation. The pressure limited capacity is then simply determined by multiplication of the maximum injection rate and the injection duration (50 years). Given the base case parameters, pressure buildup can limit the storage capacity to 2.4×50 = 120 Mt for the probable boundary scenario of impermeable Romeleåsen fault zone. For the scenario of all faults impermeable, the storage capacity becomes 80 Mt. If the formation permeability is 400 mD, the storage capacity for the scenario of impermeable Romeleåsen Fault Zone increases considerably to 415 Mt.

5. Discussion and concluding remarks

In this study, we have extended a semi-analytical solution [19,23] for application to estimate pressure buildup and maximum injection rate of CO_2 at a field site (South Scania, Sweden) using the method of superposition of image well solutions. The site is characterized by three major faults formed into a triangular geometry. The semi-analytical approach for estimating pressure buildup has been validated by comparison to numerical simulations based on TOUGH2-ECO2N for the case of closed boundaries. We have tested injection pressure sensitivity due to uncertainty in reservoir parameters as well as boundary conditions. Maximum injection rates and pressure limited capacity

estimates based on the modeling results are presented. This work demonstrates the use of semi-analytical solutions to analyze pressure limitation on storage capacity for realistic reservoirs with irregular (non-circular) boundaries. The methodology is useful for screening analysis of storage sites as well as for operation design and optimization where pressure buildup as a limiting factor influences the objective function.

The semi-analytical solution is based on one-dimensional, two-phase, two-component radial flow. It takes into account both the effect of mutual solubility between CO_2 and brine and the effect of relative permeabilities. Since it is based on one-dimensional equations, CO_2 migration due to buoyancy is ignored. For evenly distributed injection rates along the formation thickness, buoyancy flow of CO_2 would cause the pressure buildup to be higher at the top of the formation. However, this effect should be small (maximum a few bars, given the thickness of the formation and the density difference between CO_2 and brine) compared to the threshold pressure increase of $\sim 10^2$ bars.

Parametric sensitivity study using the semi-analytical model shows that the pressure buildup for the case of single injection well is very sensitive to the formation transmissivity (permeability and thickness) and boundary conditions. However, in many field sites, permeability is largely uncertain due to heterogeneity and data scarcity. Also, uncertainty can often exist in the boundaries conditions associated with the fault zones. This means that appraisal of the practical storage capacity under the pressure constraint should give uncertainty bounds, which can be obtained using the semi-analytical approach.

For closed reservoirs, the semi-analytical approach can also be used to evaluate the benefit of having more injection wells in terms of increasing the injection pressure

limited storage capacity. This is demonstrated for the South Scania site with the impermeable faults scenario. Here, the reservoir domain is conceptualized as consisting of individual parts with a closed circular boundary for each injection well. The controlling factor for the effect of number of injection wells is the hydraulic diffusivity D_h. If D_h is small (propagation distance of the pressure perturbation during the injection period is small), increasing the number of injection wells leads to increased storage capacity, although the additional operation cost needs also to be considered in the storage project implementation.

It is worth noting that we have assumed impermeable sealing units for the storage formation. In fact, the injection-induce pore pressure can be dissipated by brine storage in and displacement through the caprock if the permeability of the caprock is not extremely low and the compressibility of the caprock is large. [14] Thus, accounting for the effect of caprock and baserock could result in smaller pressure buildup and larger injection rates, depending on the relevant parameters of the sealing units. In this regard, the pressure limited capacity estimates for the South Scania site may be conservative. We are currently working on extending the semi-analytical solution to account for the pressure dissipation due to sealing rocks.

Storage capacity can be constrained both by pressure buildup and long term CO_2 plume migration to undesirable locations such as conducting faults and outcrop regions (e.g., Szulczewski et al., 2014). We are carrying out dynamic modeling based on a more detailed geological model to verify if the migration (space available for trapping) constraint becomes for more dominant for a range of injection volumes.

Acknowledgment.

Funding by the European Community's Seventh Framework Programme (FP7) MUSTANG project (No 227286) and PANACEA project (No 282900) is gratefully acknowledged. The authors also thank Simon Mathias for a stimulating seminar and discussions.

References

1. Mathias SA, González Martínez de Miguel GJ, Thatcher KE and Zimmerman RW, Pressure build-up during CO_2 injection into a closed brine aquifer. *Transport Porous Med* **89**(3):383–397 (2011).
2. Birkholzer JT and Zhou QL, Basin-scale hydrogeologic mpacts of CO_2 storage: Capacity and regulatory implications. *Int J Greenhouse Gas Control* **3**(6):745–756 (2009).
3. Bradshaw J, Bachu S, Bonijoly D, Burruss R, Holloway S, Christensen NP, et al. CO_2 storage capacity estimation: Issues and development of standards. *Int J Greenhouse Gas Control* 2007 **1**(1):62–68 (2007).
4. Pruess K, Oldenburg C and Moridis G, *TOUGH2 User's Guide, version 2.0*. Lawrence Berkeley National Laboratory, Berkeley, Calif., pp. 210 (1999).
5. Pruess K, *ECO2N: A TOUGH2 Fluid Property Module for Mixtures of Water, NaCl, and CO_2*. Lawrence Berkeley National Laboratory, Berkeley, Calif. pp. 66 (2005).
6. Pruess K and Spycher N, ECO2N – A fluid property module for the TOUGH2 code for studies of CO_2 storage in saline aquifers. *Energy Convers Manag* **48**(6):1761–1767 (2007).

7. Hammond G, Lichtner PC and Lu C, Subsurface multiphase flow and multicomponent reactive transport modeling using high-performance computing, *J Phys Conf Ser* **78**(1):012025 (2007).
8. Zhou Q, Birkholzer JT, Mehnert E, Lin Y-F and Zhang K, Modeling Basin- and Plume-Scale Processes of CO_2 Storage for Full-Scale Deployment. *Ground Water* **48**(4):494–514 (2010).
9. Yamamoto H, Zhang K, Karasaki K, Marui A, Uehara H, Nishikawa N, Numerical investigation concerning the impact of CO_2 geologic storage on regional groundwater flow. *Int J Greenhouse Gas Control* **3**(5):586–599 (2009).
10. Birkholzer JT, Zhou Q and Tsang C-F, Large-scale impact of CO_2 storage in deep saline aquifers: A sensitivity study on pressure response in stratified systems. *Int J Greenhouse Gas Control* **3**(2):181–194 (2009).
11. Gasda SE, Nordbotten JM and Celia MA, Vertically averaged approaches for CO_2 migration with solubility trapping. *Water Resour Res.* **47**(5):W05528 (2011).
12. Gasda SE, Nordbotten JM and Celia MA, Application of simplified models to CO_2 migration and immobilization in large-scale geological systems. *Int J Greenhouse Gas Control* **9**:72–84 (2012).
13. Nicot J-P, Evaluation of large-scale CO_2 storage on fresh-water sections of aquifers: An example from the Texas Gulf Coast Basin. *Int J Greenhouse Gas Control* **2**(4):582–593 (2008).
14. Chang KW, Hesse MA and Nicot J-P, Reduction of lateral pressure propagation due to dissipation into ambient mudrocks during geological carbon dioxide storage. *Water Resour Res* **49**(5):2573–2588 (2013).

15. Yang Z, Niemi A, Tian L and Erlström M, Modelling of far-field pressure plumes for carbon dioxide sequestration. *Energy Procedia* **40**:472–480 (2013).
16. Person M, Banerjee A, Rupp J, Medina C, Lichtner P, Gable C et al. Assessment of basin-scale hydrologic impacts of CO_2 sequestration, Illinois basin. *Int J Greenhouse Gas Control* **4**(5):840–854 (2010).
17. Huang X, Bandilla KW, Celia MA and Bachu S, Basin-scale modeling of CO_2 storage using models of varying complexity. *Int J Greenhouse Gas Control* **20**:73–86 (2014).
18. Dentz M, and Tartakovsky DM, Abrupt-interface solution for carbon dioxide injection into porous media. *Transport Porous Med* **79**(1):15–27 (2008).
19. Mathias SA, Gluyas JG, González Martínez de Miguel GJ and Hosseini SA, Role of partial miscibility on pressure buildup due to constant rate injection of CO_2 into closed and open brine aquifers. *Water Resour Res* **47**(12):W12525 (2011).
20. Nordbotten JM, Celia MA and Bachu S, Injection and storage of CO_2 in deep saline aquifers: Analytical solution for CO_2 plume evolution during injection. *Transport Porous Med* **58**(3):339–360 (2005).
21. Vilarrasa V, Bolster D, Dentz M, Olivella S and Carrera J, Effects of CO_2 compressibility on CO_2 storage in deep saline aquifers. *Transport Porous Med* **85**(2):619–639 (2010).
22. Vilarrasa V, Carrera J, Bolster D and Dentz M, Semianalytical solution for CO_2 plume shape and pressure evolution during CO_2 injection in deep saline formations. *Transport Porous Med* **97**(1):43–65 (2013).

23. Mathias SA, Gluyas JG, González Martínez de Miguel GJ, Bryant SL and Wilson D, On relative permeability data uncertainty and CO_2 injectivity estimation for brine aquifers. *Int J Greenhouse Gas Control* **12**:200–212 (2013).
24. Castelletto N, Gambolati G and Teatini P. Geological CO2 sequestration in multi-compartment reservoirs: Geomechanical challenges. *J Geophys Res Solid Earth* **118**:2417–2428 (2013).
25. Rutqvist J, Birkholzer J, Cappa F and Tsang C-F, Estimating maximum sustainable injection pressure during geological sequestration of CO2 using coupled fluid flow and geomechanical fault-slip analysis. *Energy Convers Manag* **48**(6):1798–1807 (2007).
26. Rutqvist J, Birkholzer JT and Tsang C-F, Coupled reservoir–geomechanical analysis of the potential for tensile and shear failure associated with CO_2 injection in multilayered reservoir–caprock systems. *Int J Rock Mech Min Sci* **45**(2):132–143 (2008).
27. Vilarrasa V, Bolster D, Olivella S and Carrera J, Coupled hydromechanical modeling of CO_2 sequestration in deep saline aquifers. *Int J Greenhouse Gas Control* **4**(6):910–919 (2010).
28. Morris JP, Detwiler RL, Friedmann SJ, Vorobiev OY and Hao Y, The large-scale geomechanical and hydrogeological effects of multiple CO_2 injection sites on formation stability. *Int J Greenhouse Gas Control* **5**(1):69–74 (2011).
29. Mathias SA, Hardisty PE, Trudell MR and Zimmerman RW, Screening and selection of sites for CO_2 sequestration based on pressure buildup. *Int J Greenhouse Gas Control* **3**(5):577–585 (2009).

30. Altunin, VV, *Thermophysical Properties of Carbon Dioxide*. Publishing House of Standards, Moscow (1975).
31. Chasset C, Jarsjö J, Erlström M, Cvetkovic V and Destouni G, Scenario simulations of CO_2 injection feasibility, plume migration and storage in a saline aquifer, Scania, Sweden. *Int J Greenhouse Gas Control* **5**(5):1303–1318 (2011).
32. Krevor SCM, Pini R, Zuo L and Benson SM, Relative permeability and trapping of CO_2 and water in sandstone rocks at reservoir conditions. *Water Resour Res* **48**(2):1–16 (2012).
33. Brooks RH and Corey AT, Hydraulic properties of porous media, Hydrogeology papers. Colorado State University, Fort Collins, Colorado, pp. 27 (1964).
34. Burdine, NT, Relative permeability calculations from pore size distribution data, *Trans. AIME* **198**:71 (1953).
35. Yang Z, Tian L, Niemi A and Fagerlund F, Upscaling of the constitutive relationships for CO_2 migration in multimodal heterogeneous formations. *Int J Greenhouse Gas Control* **19**:743–55 (2013).
36. Erlström M, Silva O, de Vries LM, Shtivelman V, Gendler M, I. Goldberg et al. 3D structures of test sites. *EU FP7 MUSTANG Project Report D022*, http://www.co2mustang.eu/MustangDeliverables.aspx /[accessed 20 December 2010]
37. Ferris JG, Knowles DB, Brown RH and Stallman RW, Theory of aquifer tests, U.S. Geological Survey Water-Supply Paper 1536-E (1962).

38. Tsang C-F, Birkholzer J and Rutqvist J, A comparative review of hydrologic issues involved in geologic storage of CO_2 and injection disposal of liquid waste. *Environ Geol* **54**(8):1723–1737 (2008).
39. Ringrose PS, Martinius AW and Alvestad J, Multiscale geological reservoir modelling in practice. *Geological Society London Special Publications* **309**(1):123-134 (2008).
40. Burton M, Kumar N and Bryant SL, CO_2 injectivity into brine aquifers: Why relative permeability matters as much as absolute permeability. *Energ Procedia* **1**(1):3091–3098 (2009).
41. Szulczewski ML, MacMinn CW and Juanes R, Theoretical analysis of how pressure buildup and CO_2 migration can both constrain storage capacity in deep saline aquifers. *Int J Greenhouse Gas Control* **23**:113–118 (2014).

Table 1. Sensitivity of maximum injection rate (Mt/yr) to parameters and boundary conditions.

Parameter	Romeleåsen Fault impermeable	All faults impermeable
k = 25 mD	0.68	0.59
50 mD	1.3	0.98
100 mD *	2.4	1.6
400 mD	8.3	2.8
φ = 0.1	2.3	1.4
0.15 *	2.4	1.6
0.2	2.5	1.7
0.25	2.5	1.9
$c_r = 4.5\times10^{-9}$ Pa^{-1}	2.2	1.3
4.5×10^{-10} Pa^{-1} *	2.4	1.6
4.5×10^{-11} Pa^{-1}	3.1	2.8
H = 50 m	1.6	1.1
75 m *	2.4	1.6
100 m	3.2	2.2
150 m	4.8	3.2

* Base case parameters

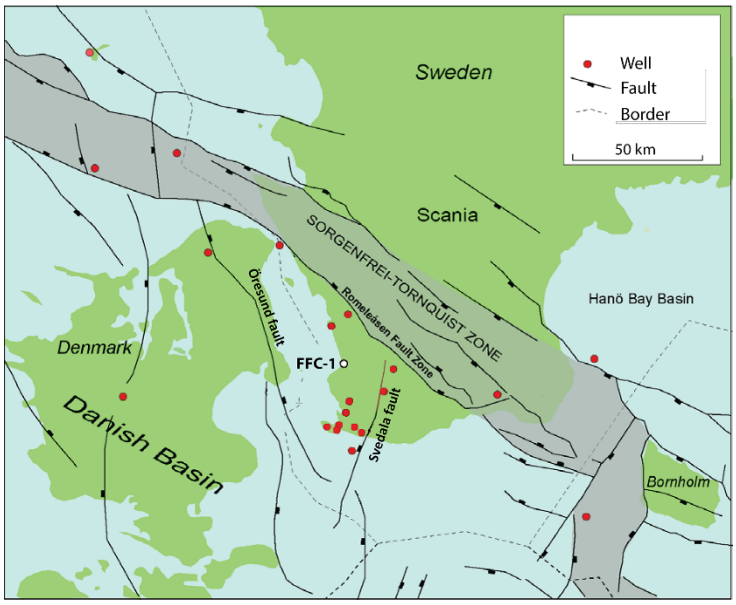

Fig. 1. Map of the South Scania site, Sweden.

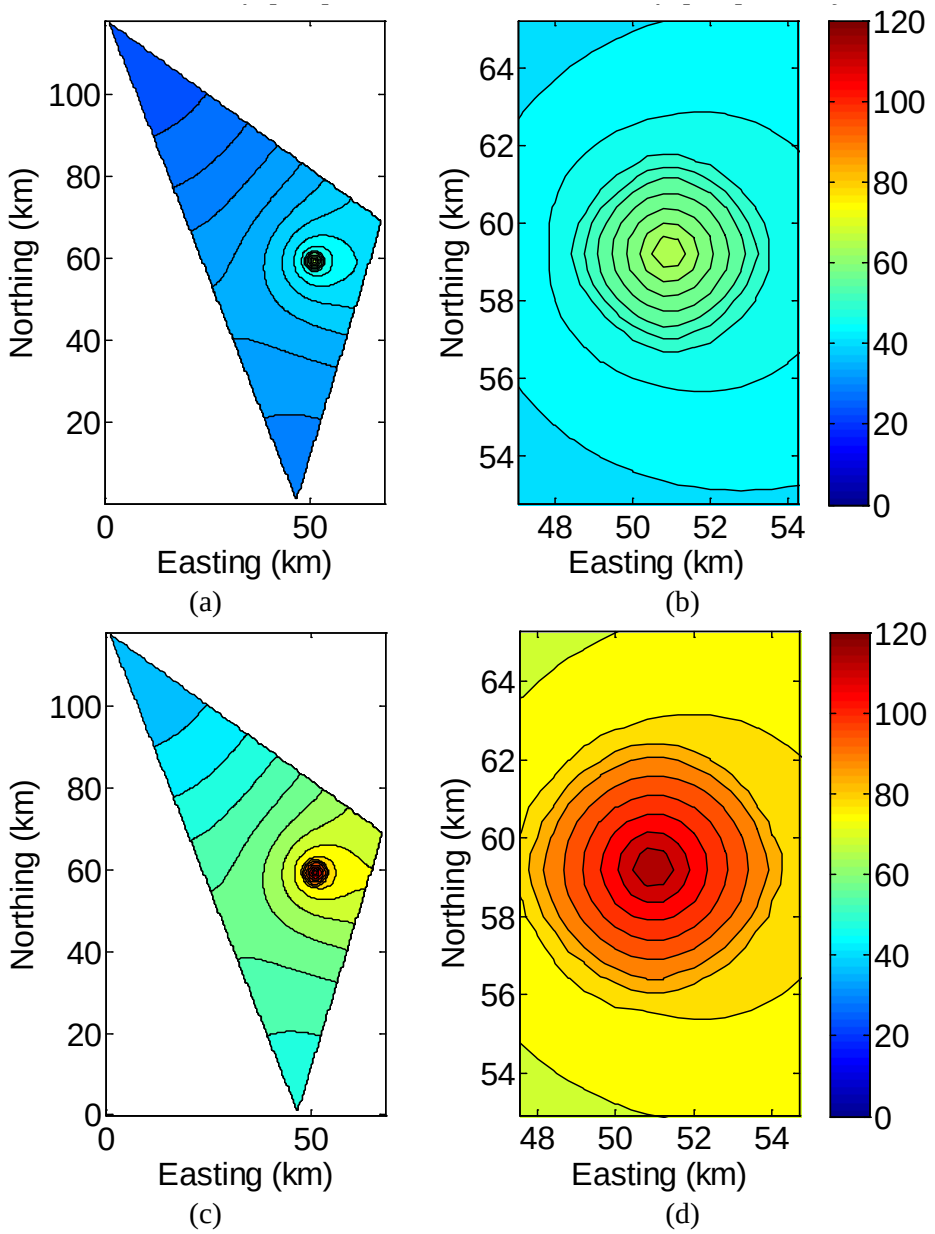

Fig. 2. (a) Numerically simulated pressure increase (bar) at 50 years with CO_2 injection rate 1 Mt/yr. (b) Zoom-in view (CO_2 injection rate 1 Mt/yr). (c) Numerically simulated pressure increase (bar) with CO_2 injection rate 2 Mt/yr. (b) Zoom-in view (CO_2 injection rate 2 Mt/yr).

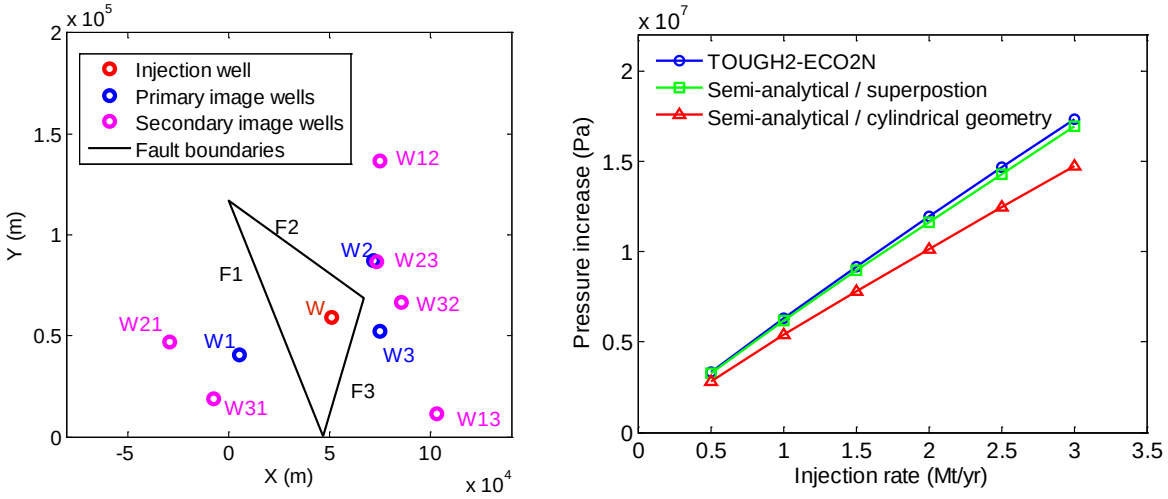

(a) (b)

Fig. 3. (a) Reservoir modeling domain with fault boundaries and locations of the injection well and image wells. Primary image well W_i is the image of injection well with respect to fault F_i; Secondary image well W_{ij} is the image of primary image well W_i with respect to fault F_j; (b) Comparison of pressure prediction between numerical modeling and analytical solutions.

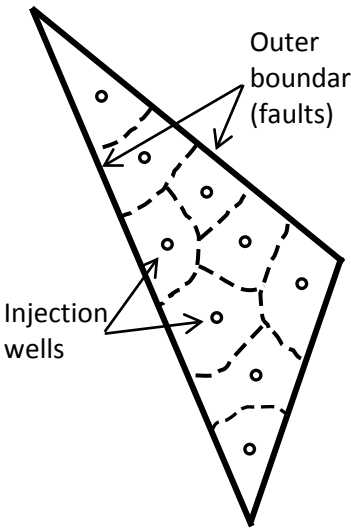

Fig. 4. Schematic showing the divided reservoir domain with the scenario of multiple injection wells.

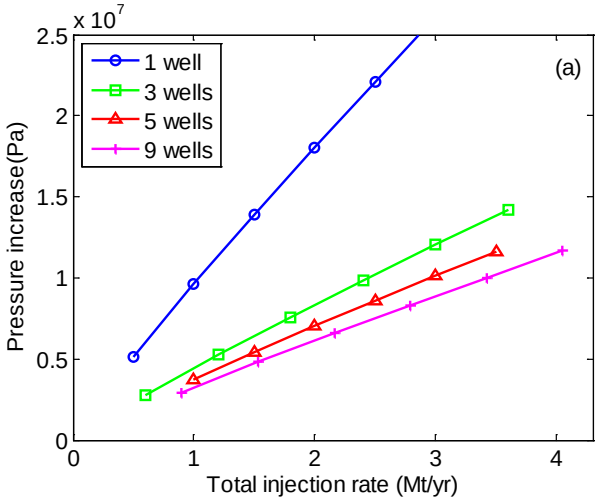

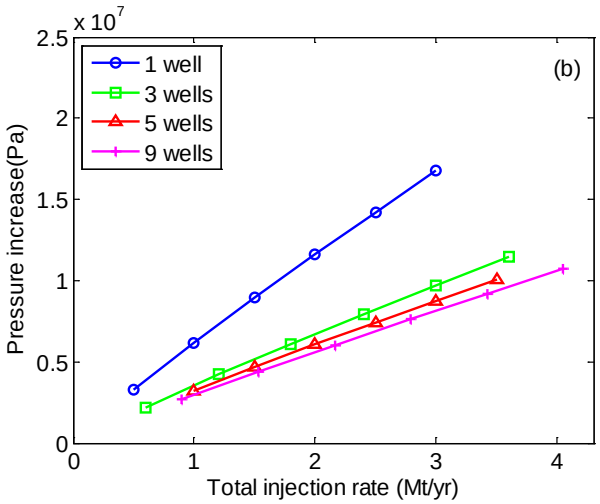

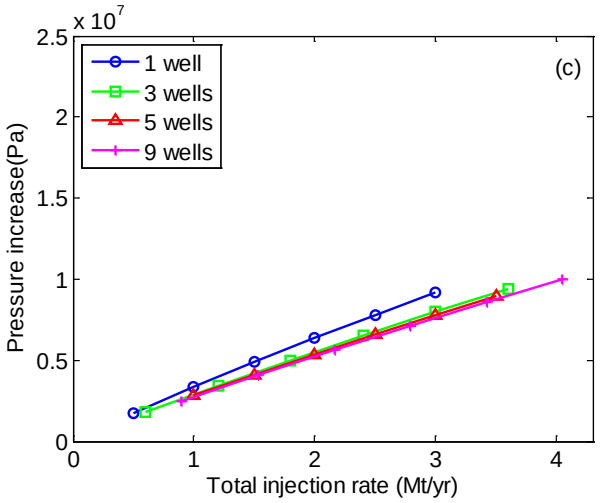

Fig. 5. Well pressure increase for different number of injection wells with evenly distributed injection rates. (a) permeability 50 mD; (b) permeability 100 mD; (c) permeability 400 mD.

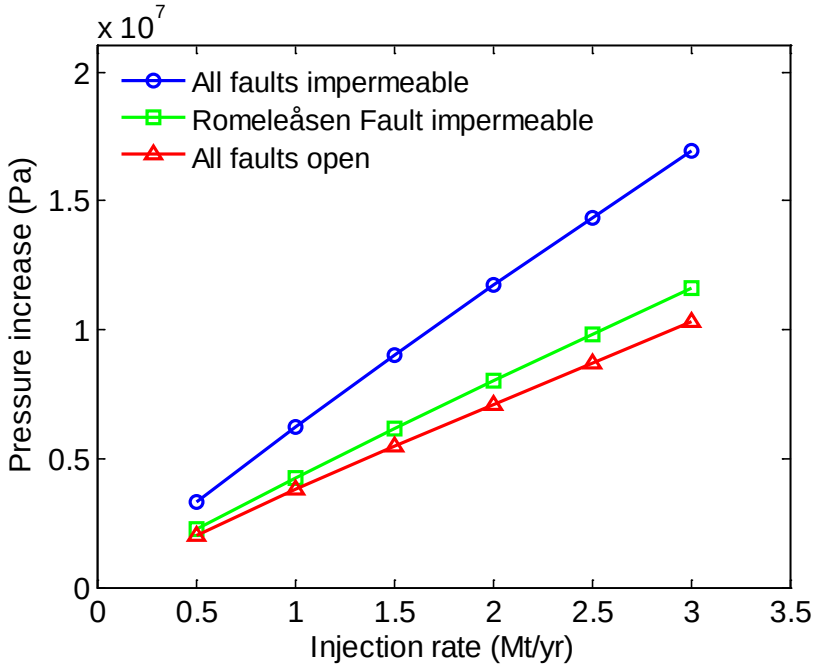

Fig. 6. Effect of boundary conditions on the injection pressure.

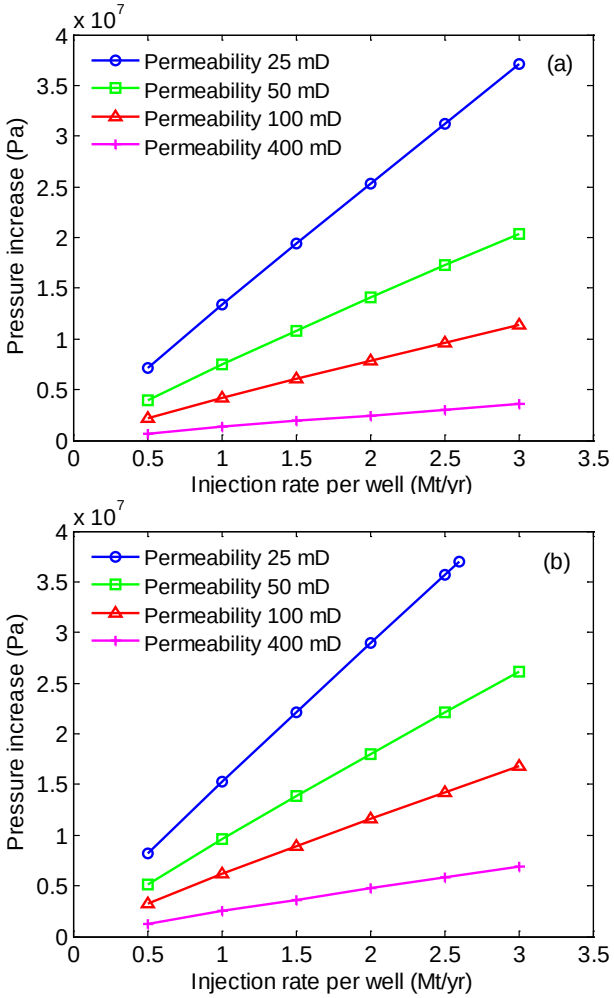

Fig. 7. Sensitivity of pressure buildup on permeability variation. (a) Romeleåsen Fault impermeable; (b) all faults impermeable.

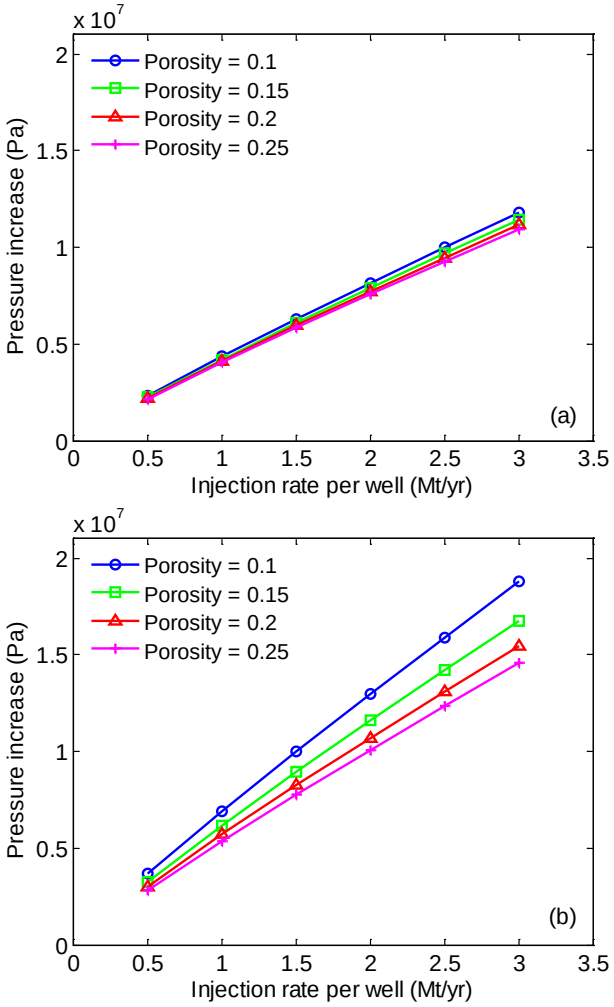

Fig. 8. Sensitivity of pressure buildup on porosity variation. (a) Romeleåsen Fault impermeable; (b) all faults impermeable.

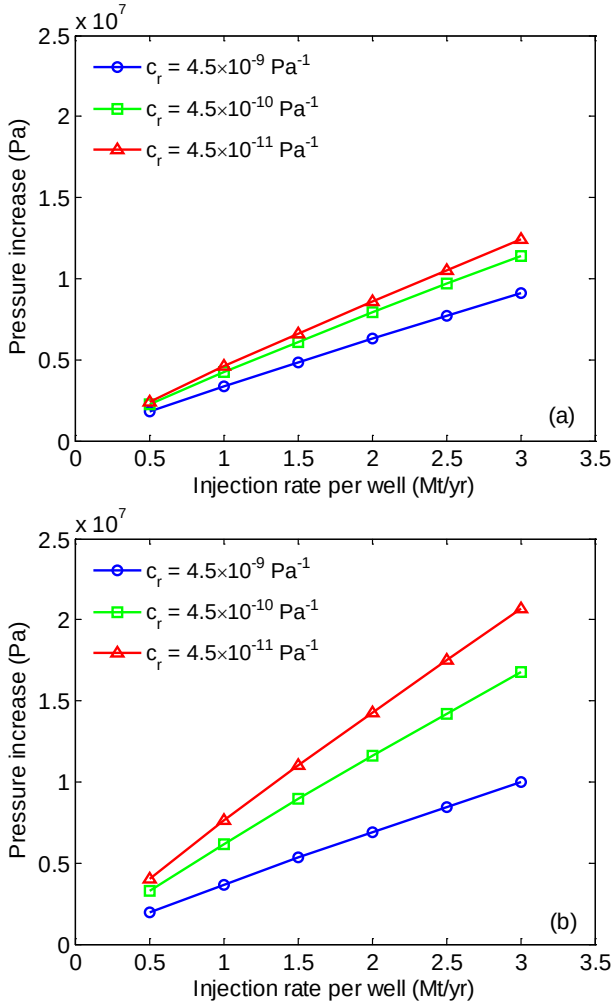

Fig. 9. Sensitivity of pressure buildup on rock compressibility variation. (a) Romeleåsen Fault impermeable; (b) all faults impermeable.

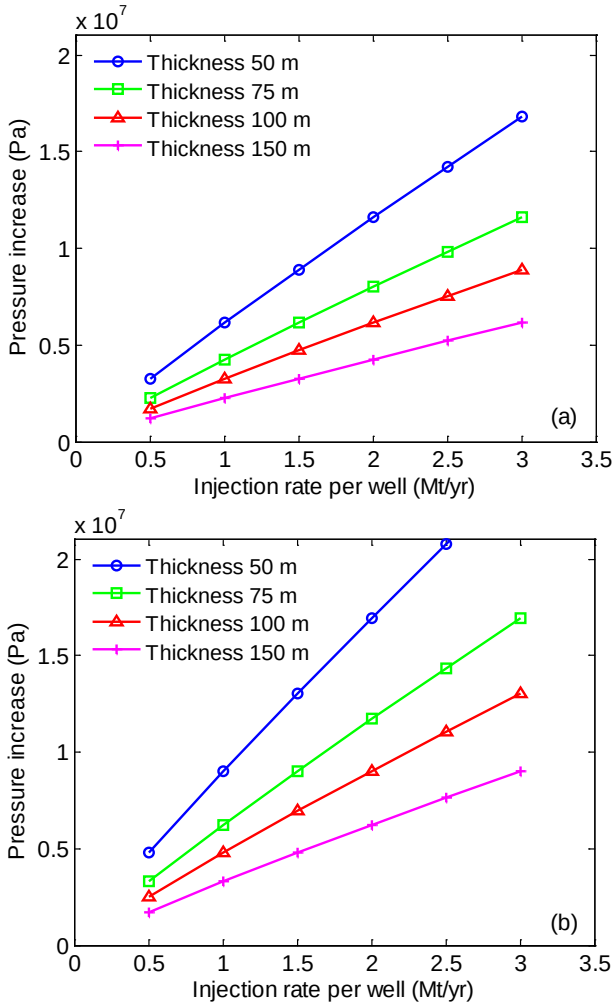

Fig. 10. Sensitivity of pressure buildup on formation thickness variation. (a) Romeleåsen Fault impermeable; (b) all faults impermeable.